Appl. Phys. A (2016) 122:374
DOI 10.1007/s00339-016-9902-4

Applied Physics A
Materials Science & Processing

Dual-resonant polarization-independent and wide-angle metamaterial absorber in X-band frequency

Osman Ayop[1] · Mohamad Kamal A. Rahim[1] · Noor Asniza Murad[1] · Noor Asmawati Samsuri[1]

Received: 13 August 2015 / Accepted: 21 November 2015 / Published online: 14 March 2016

Abstract This paper presents the analysis of dual-resonant polarization-independent metamaterial absorber with wide operating angle in X-band frequency. Two circular rings with different radius are used as resonating elements. The resonating elements which are made by copper are printed on two surfaces (top and bottom) of dual-layer FR4 substrate. At the middle layer, a full copper layer is placed. The performance of dual-resonant circular ring metamaterial absorber is observed using CST software. From simulated result, the proposed structure achieves high absorbance, which is 96.41 and 93.61 % at 9 and 11 GHz, respectively, for normal incident wave. For measurement, the resonant frequencies are found at 9.39 and 11.63 GHz with absorbance of 99.07 and 83.70 %, respectively. Then, the structure is also simulated for oblique incident angles. It is observed that the operating angle of the proposed metamaterial absorber is 70° for TE modes and 67° for TM modes. Measurement for oblique incident angle is done to validate the simulated result. Mutual agreement is achieved between simulated and measured result with slight frequency shift and ripples.

1 Introduction

Metamaterials are artificial structure, having unique properties that can be applied in many electromagnetic devices such as antennas, filters and lens. One of the interesting topics for investigation is metamaterial absorber (MMAbs). Basically, some metamaterial is used as an efficient electromagnetic reflector [1]. However, by engineering the dielectric material with metal intact, high MMAbs can be developed. Wang et al. [2] have proposed three-dimensional MMAbs that achieve high absorption for multi-directional surface. However, the operating angle of the absorber is not being observed. Landy et al. [3] proposed perfect MMAbs, but the structure is only working in single direction. Furthermore, having cut wire at the back of the structure made the analysis more difficult since the magnitudes of both reflectance and transmittance need to be controlled together to maximize the absorbance magnitude. Guo-Dong et al. [4] proposed polarization-insensitive multiband MMAbs based on coplanar Jerusalem crosses. However, to achieve a multiband frequency, multiple sizes of resonating elements are needed because each size can only provide one resonant frequency. Hu et al. [5] proposed quad-band MMAbs based on electric LC resonator (ELCR) and metal cross. The structure is designed in dual layer; however, it can only absorb EM wave in single direction. Guo et al. [6] proposed triple-band wide-angle MMAbs based on regular pentagon closed ring. The proposed structure is insensitive to all polarization angles and works at very large operating angle. However, to achieve such excellent performance, three layers are needed where it can increase the overall size and fabrication cost. Kim et al. [7] proposed dual-broadband MMAbs based on metal–dielectric multilayer truncated cones. The proposed structure is insensitive to all polarization angles and works very well at incident angle up to 45°. However, the design is rather complicated because multilayer metal–dielectric is needed in the form of truncated cones. The overall thickness is also increased.

✉ Mohamad Kamal A. Rahim
mkamal@fke.utm.my

[1] Advanced RF and Microwave Research Group, Department of Communication Engineering, Faculty of Electrical Engineering, Universiti Teknologi Malaysia, FKE, UTM, Johor Bahru 81310, Johor, Malaysia

2 Proposed design, simulation, fabrication, measurement and discussion

This paper proposed a polarization-insensitive MMAbs which can operate at very wide incident angle and provides two resonant frequencies. At the same time, the structure can absorb the incident of EM waves coming from two directions (+z and −z) because the resonating elements are printed at both surfaces of dielectric substrate. The substrate used in this design is FR4 substrate which has dielectric constant of 4.6, loss tangent of 0.019 and thickness of 0.8 mm. The resonating elements are made by 0.035-mm-thick copper with a conductivity of 5.8×10^7 S/m. CST software is used to simulate the structure. The optimized design is fabricated using standard PCB etching technique. Then, the measurement of fabricated structure is done in X-band anechoic chamber room as shown in Fig. 1. From the figure, it shows that two standard gain horn antennas are used for transmitting and receiving the EM waves. A semicircle-shaped track is used to hold the horn antennas at specific angle during measurement. The MMAbs are placed at the centre point of the arc circle during measurement. The X-band broadband triangle absorbers are used to absorb unwanted EM wave that may affect the measurement result. A vector network analyser (VNA) is used to measure the reflection of EM wave on the sample of MMAbs. Before conducting the simulation, the dimension of MMAbs is calculated using Eqs. (1)–(3):

$$r = \frac{\lambda_{go}}{2\pi} = \frac{\lambda_o}{2\pi\sqrt{\varepsilon_{re}}} = \frac{300}{2\pi f_o(\mathrm{GHz})\sqrt{\varepsilon_{re}}} \quad (1)$$

$$\varepsilon_{re} = \frac{\varepsilon_r + 1}{2} + \frac{\varepsilon_r - 1}{2}\left(\left(1 + 12\frac{h}{w_r}\right)^{0.5} + 0.04\left(1 - \frac{w_r}{h}\right)^2\right) \quad (2)$$

$$f_o = \frac{300}{\pi(r_o + r_i)\sqrt{\varepsilon_{re}}} \quad (3)$$

where r = radius of circular ring, r_o = outer radius of circular ring, r_i = inner radius of circular ring, λ_{go} = guided wavelength at resonant, and ε_{re} = effective relative permittivity.

However, due to coupling effect that may exist between two circular rings, the result from simulation is slightly away from expected. Therefore, the dimension of the structure is optimized to obtain the absorbance at desired resonant frequencies.

2.1 Proposed dual-resonant metamaterial absorber

The design of dual-resonant CRMMAbs is illustrated in Fig. 2. The corresponding dimensions are listed in Table 1. The dimension of the unit cell ($W \times L \times h$) is approximately $3\lambda_g/5 \times 3\lambda_g/5 \times \lambda_g/10$ referring to the λ_g of the element with highest resonant frequency. The average radius of resonating elements, r_1 and r_2, is close to $\lambda_g/6$

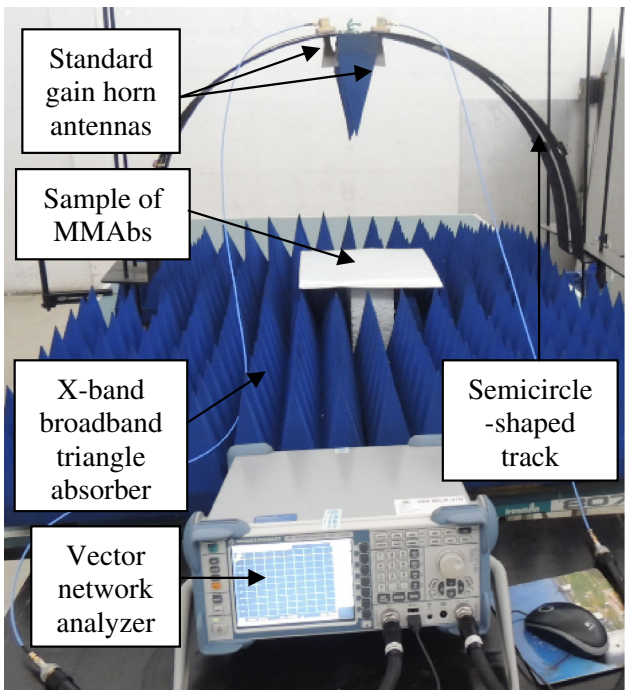

Fig. 1 Measurement set-up for MMAbs in X-band anechoic chamber room

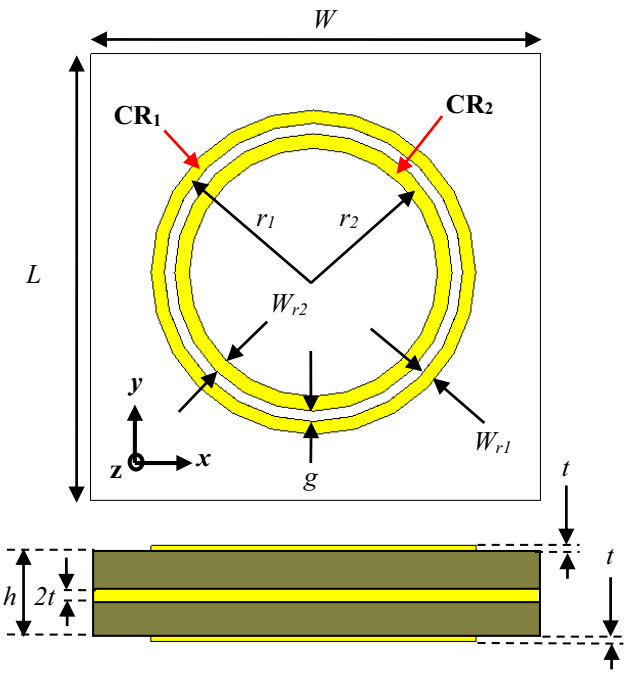

Fig. 2 The proposed structure of dual-resonant MMAbs

Table 1 Dimension of dual-resonant CRMMAbs

Parameter	Dimension (mm)	Dimension in λ_g at resonance
W, L	9.000	$0.584\lambda_g$
r_1	2.510	$0.163\lambda_g$
r_2	2.975	$0.158\lambda_g$
W_{r1}	0.250	$0.016\lambda_g$
W_{r2}	0.280	$0.018\lambda_g$
g	0.200	$0.013\lambda_g$
h	1.670	$0.108\lambda_g$
t	0.035	$0.002\lambda_g$

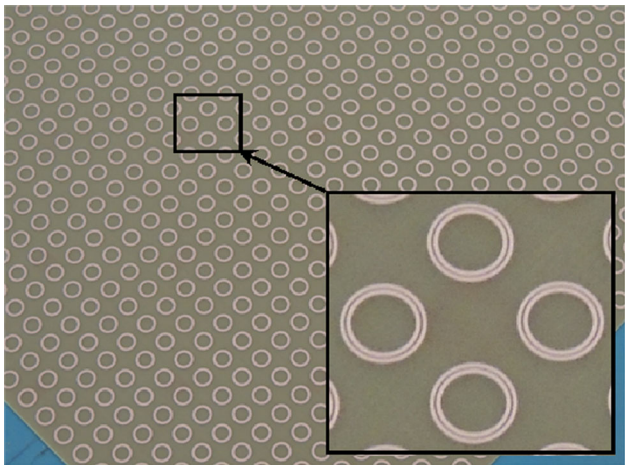

Fig. 3 Fabricated dual-resonant CRMMAbs

referring to their own λ_g at resonant frequency. The width of the resonating elements, W_{r1} and W_{r2}, is nearly $\lambda_g/55$ and $\lambda_g/60$, respectively. The gaps between two resonating elements, g, is $\lambda_g/80$. All the dimensions of the structure are listed in Table 1. When observing the physical dimension of the proposed MMAbs, it is very thin compared to the operating wavelength. Metamaterial structure is well known as an artificial structure which can be scaled much smaller compared to the operating wavelength. Therefore, the mechanism of the structure can be analysed using equivalent lump-element circuit. The structure is then fabricated based on the optimized result obtained from simulation. The fabricated structure is depicted in Fig. 3. It consists of 1089 resonating elements at each surface of 300 × 300 mm FR4 substrate. A copper layer is sandwiched between two dielectric substrates.

2.2 Performance of dual-resonant CRMMAbs for normal incident of EM wave

The simulated reflectance, transmittance and absorbance of dual-resonant CRMMAbs are shown in Fig. 4. The

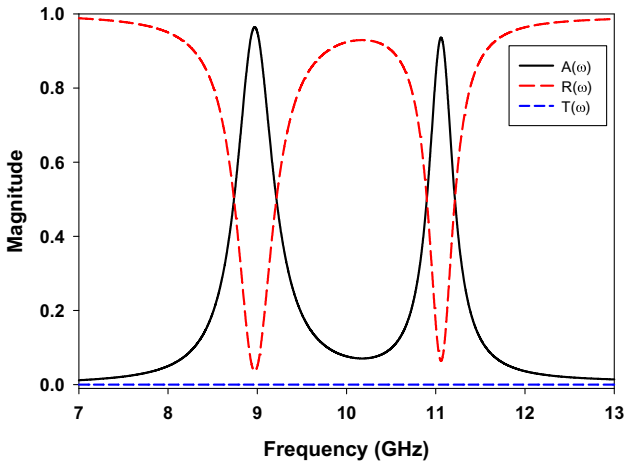

Fig. 4 Simulated transmittance, reflectance and absorbance of dual-resonant CRMMAbs

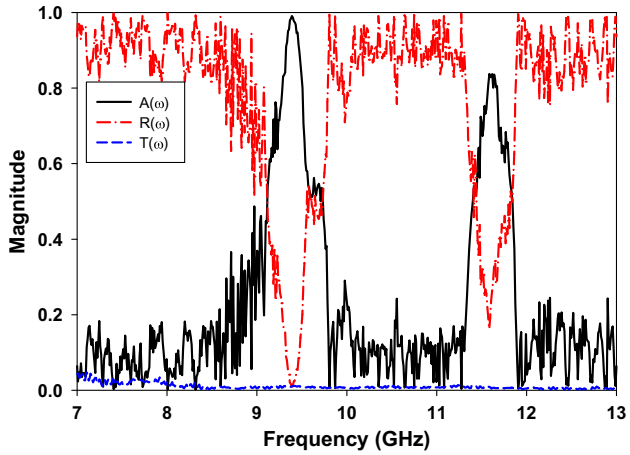

Fig. 5 Measured transmittance, reflectance and absorbance of dual-resonant CRMMAbs

transmittance, $T(\omega)$, is zero for all frequencies due to the full copper layer at the middle between two substrates. The absorbance, $A(\omega)$, is determined by reflectance, $R(\omega)$, magnitude only. For normal incident wave, $R(\omega)$ are 4.89 and 16.56 % so that $A(\omega)$ are 95.11 and 83.44 % at 9 and 11 GHz, respectively. The corresponding FWHM bandwidths are 5.24 % (8.74–9.21 GHz) and 2.80 % (10.90–11.21 GHz). The absorbance at two resonant frequencies is above 80 %, indicating that high absorbance is achieved.

The measured $T(\omega)$, $R(\omega)$ and $A(\omega)$ are presented in Fig. 5. As expected, the $T(\omega)$ is almost zero for all measured frequencies due to the full metal plane at the middle between two substrates. The $R(\omega)$ is minimized at two resonance frequencies of 9.39 and 11.62 GHz with magnitude of 0.93 and 16.30 %, respectively. Hence, $A(\omega)$ become 99.07 and 83.70 %. The FWHM bandwidths are 6.57 % (9.12–9.74 GHz) and 3.77 % (11.40–11.84 GHz),

respectively. The result shows that a good agreement is achieved between simulation and measurement with a slight frequency shift may be due to the variation of substrate effective permittivity at high frequency. However, the noise in the measured response is due to measurement set-up and tolerance.

2.3 Performance of dual-resonant CRMMAbs for oblique incident of EM wave

Figure 6 plots the graph of simulated absorbance for TE polarization incident EM waves. The magnitude of $A(\omega)$ for dual-resonant CRMMAbs is observed every 20° step angle between 0° and 60°. It is observed that for the first resonant, the $A(\omega)$ remain very high up to 60° which is more than 95 %. However, for the second resonant, the $A(\omega)$ decreased to 66.94 %. Next, the incident angle is altered until the $A(\omega)$ become at least 50 %. It is observed that the operating angle for TE mode, $\theta_{\mathrm{mTE}} = 70°$. It is observed that the $A(\omega)$ for second resonant decreased rapidly and become around 50 % at 70°. Contrarily, the first resonant still manages to achieve $A(\omega) = 85.51$ % for the same incident angle. The exact resonant frequencies and their corresponding $A(\omega)$ are listed in Table 2. It shows that the resonant frequency for the first resonant varies between 8.97 and 9.10 GHz ($\Delta f_{\mathrm{r1}} = 0.13$ GHz). For second resonant, it varies between 10.95 and 11.22 GHz ($\Delta f_{\mathrm{r2}} = 0.27$ GHz).

The absorbing mechanism of the metamaterial absorber is based on the impedance matching between the absorber and the free space impedance. To obtain perfect absorption, the effective permittivity, $\varepsilon(\omega)$, must be in the same magnitude with effective permeability, $\mu(\omega)$, which mean that the electric and magnetic resonant must be obtained simultaneously. For TE polarization, the electric component of the incident EM wave is always parallel with the surface of absorber so that electric resonant can be obtained. However, the excitation angle of magnetic component is varied. As the excitation angle increases, the ability of magnetic field to penetrate the substrate and to drive the magnetic flux inside the substrate is reduced. Therefore, the magnetic resonance becomes less and causes the impedance mismatch.

Table 2 The detail simulated absorbance of dual-resonant CRMMAbs in TE polarization

Incident angle (θ°)	First resonant		Second resonant	
	Frequency (GHz)	A(ω) (%)	Frequency (GHz)	A(ω) (%)
0	9.00	95.11	11.00	83.43
20	8.97	97.65	10.95	77.79
40	9.04	99.76	11.12	81.59
60	9.06	95.70	11.13	66.94
67	9.09	85.51	11.20	51.03
82	9.10	51.20	11.22	23.47

Figure 7 plots the graph of measured absorbance of dual-resonant CRMMAbs for TE polarization incident EM waves between 0° and 60°. The measurement is not conducted for incident angle more than 60° because the measurement will not be valid due to the direct coupling between transmitted and received antennas. The $A(\omega)$ and its corresponding resonant frequencies are listed in Table 3. It is observed that at 60° the $A(\omega)$ for the first resonant frequency remain greater than 92 %, while for second resonant frequency, $A(\omega)$ is greater than 53.30 %. Similarly, resonant frequencies vary slightly when the incident angle increased as predicted in simulation result. Similar pattern is observed between simulation and measurement, but a slight frequency shift and ripples are found in measurement.

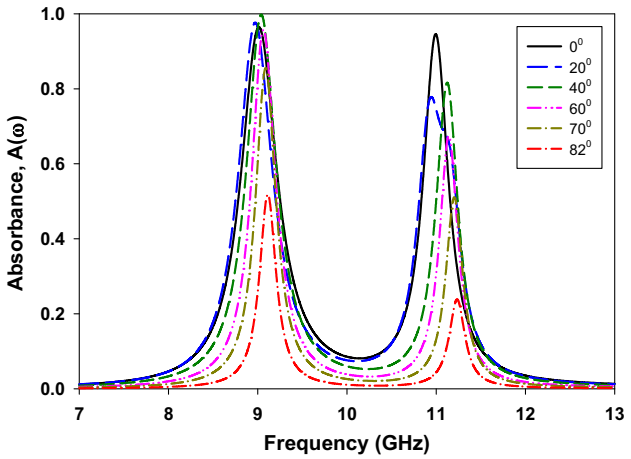

Fig. 6 Simulated absorbance, $A(\omega)$ for TE polarization of incident EM wave

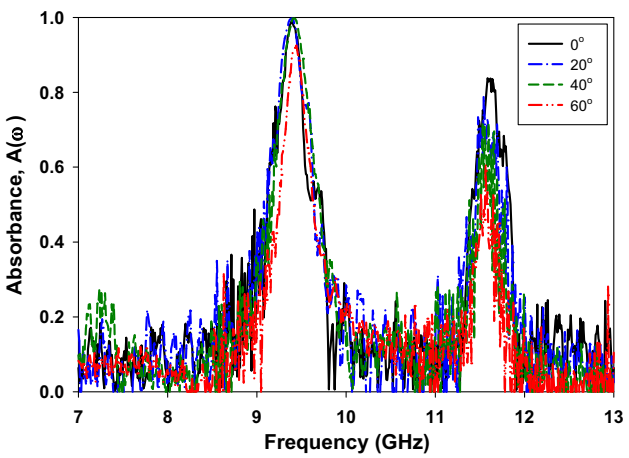

Fig. 7 Measured absorbance, $A(\omega)$ for TE polarization of incident EM wave

Table 3 The detail measured absorbance of dual-resonant CRMMAbs in TE polarization

Incident angle (θ^o)	First resonant		Second resonant	
	Frequency (GHz)	A(ω) (%)	Frequency (GHz)	A(ω) (%)
0	9.39	99.07	11.62	83.70
20	9.39	99.72	11.54	78.96
40	9.41	99.73	11.53	71.92
60	9.44	92.53	11.59	53.30

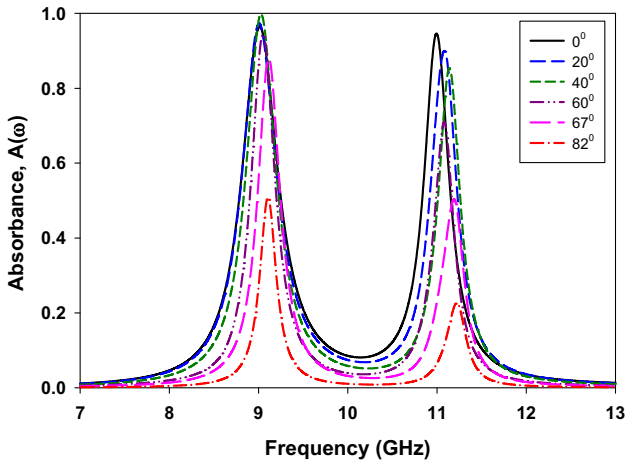

Fig. 8 Simulated absorbance, $A(\omega)$ for TM polarization of incident EM wave

Next, the simulated absorbance of dual-resonant CRMMAbs for TM polarization incident EM waves is presented. The result is plotted in Fig. 8. Similar to TE polarization, the magnitude of $A(\omega)$ is observed every 20° step angle between 0° and 60°. Similar to TE mode, the $A(\omega)$ remain very high up to 60° which is more than 94 %. However, for the second resonant, the $A(\omega)$ decreased to 70.98 %. The operating angle in which the $A(\omega)$ can maintain at least 50 % for TM mode, $\theta_{\mathrm{mTM}} = 67°$ due to the rapid decrement for the second resonant. Contrarily, the first resonant still manages to achieve $A(\omega) = 87.95$ % for the same incident angle. The detail $A(\omega)$ and its corresponding resonant frequency are given in Table 4. It shows that the resonant frequency for the first resonant varies between 9.01 and 9.11 GHz ($\Delta f_{\mathrm{r1}} = 0.10$ GHz). For second resonant, it varies between 10.99 and 11.22 GHz ($\Delta f_{\mathrm{r2}} = 0.23$ GHz). For TM polarization, the magnetic component of EM wave is always parallel with the surface of the absorber, while the electric component is varied. The magnetic resonant can be obtained under different excitation angles under TM polarization. However, the electric component which provides electric resonant becomes less effective under large excitation angle of incident EM wave and causes the impedance mismatch.

Table 4 The detail simulated absorbance of dual-resonant CRMMAbs in TM polarization

Incident angle ($\theta°$)	First resonant		Second resonant	
	Frequency (GHz)	A(ω) (%)	Frequency (GHz)	A(ω) (%)
0	9.01	96.43	10.99	94.55
20	9.01	97.29	11.09	89.80
40	9.03	99.79	11.14	85.35
60	9.05	94.50	11.08	70.98
67	9.11	87.95	11.19	50.40
82	9.11	50.79	11.22	22.64

The electric resonant can be seen from the flow of currents which is going upward and downward alternately from upper half to lower half of the circular ring resonator. The flow of currents is like a dipole moment.

Figure 9 plots the graph of measured absorbance of dual-band CRMMAbs for TM polarization incident EM waves between 0° and 60° incident angle. The $A(\omega)$ and its corresponding resonant frequency are given in Table 5. The pattern of the graph follows the simulated results with a slight frequency shift. It is observed that up to 60°, the magnitudes of $A(\omega)$ for first resonant frequency are greater than 96 % and for second resonant frequency are greater than 79 %.

2.4 Field distribution and surface currents

Next, the field distribution and surface currents of dual-resonant CRMMAbs are investigated at resonant frequencies. Since the proposed design has two resonant frequencies, the simulation is conducted at both frequencies which are 9 and 11 GHz, respectively.

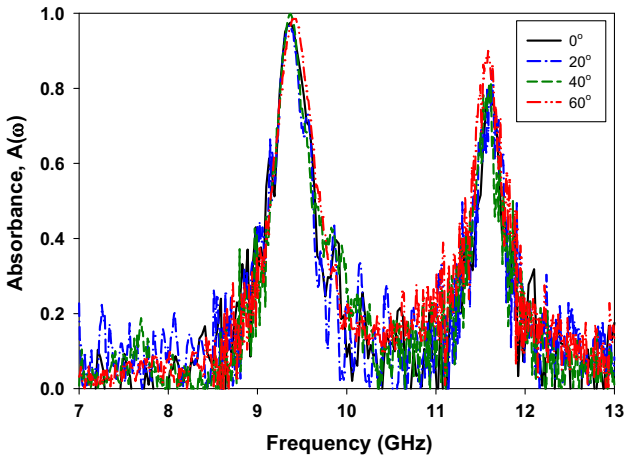

Fig. 9 Measured absorbance, $A(\omega)$ for TM polarization of incident EM wave

Table 5 The detail measured absorbance of dual-resonant CRMMAbs in TM polarization

Incident angle (θ°)	First resonant		Second resonant	
	Frequency (GHz)	A(ω) (%)	Frequency (GHz)	A(ω) (%)
0	9.37	97.52	11.59	79.29
20	9.35	96.92	11.63	84.73
40	9.37	99.88	11.62	81.04
60	9.40	98.51	11.59	90.00

To start with, the simulated E-field distribution in Fig. 10a, c will be discussed. At 9 GHz, the E-field distribution is very strong at g between CR_1 and CR_2 that is located vertically. This indicates that strong electric coupling exists between two parallel metal elements. Strong E-field is also observed at the outer side near CR_1 which indicates that CR_1 contributes to the lower resonant. The E-field distribution becomes weaker when approaching the horizontal part of the structure. At 11 GHz, strong E-field distribution is also observed at g which indicates that electric coupling is also applied at the same place for higher resonant frequency. Some significantly high magnitude of E-field is also observed at the outer side near CR_2 which indicates that CR_2 contributes to the higher resonant.

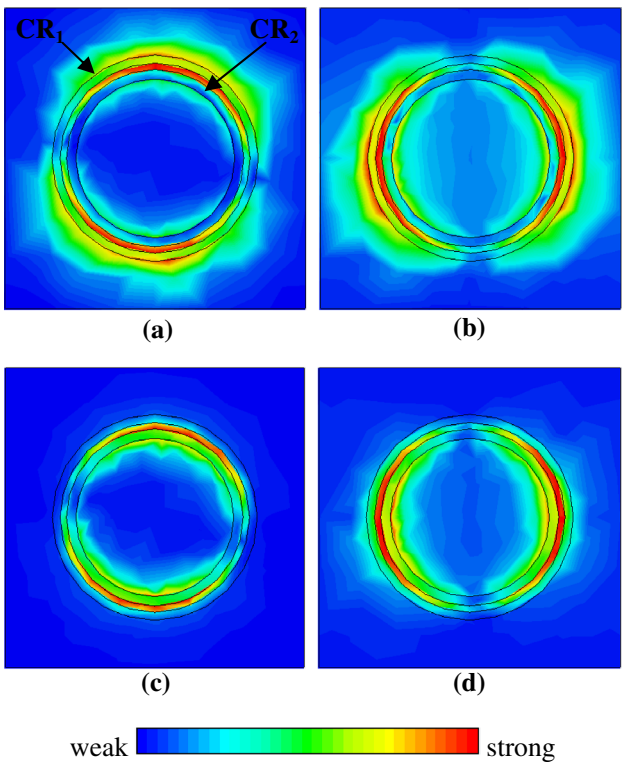

Fig. 10 Simulated E-field and H-field distribution at 9.00 and 11.00 GHz. **a** E-field at $f = 9.00$ GHz, **b** H-field at $f = 11.00$ GHz, **c** E-field at $f = 9.00$ GHz, **d** H-field at $f = 11.00$ GHz

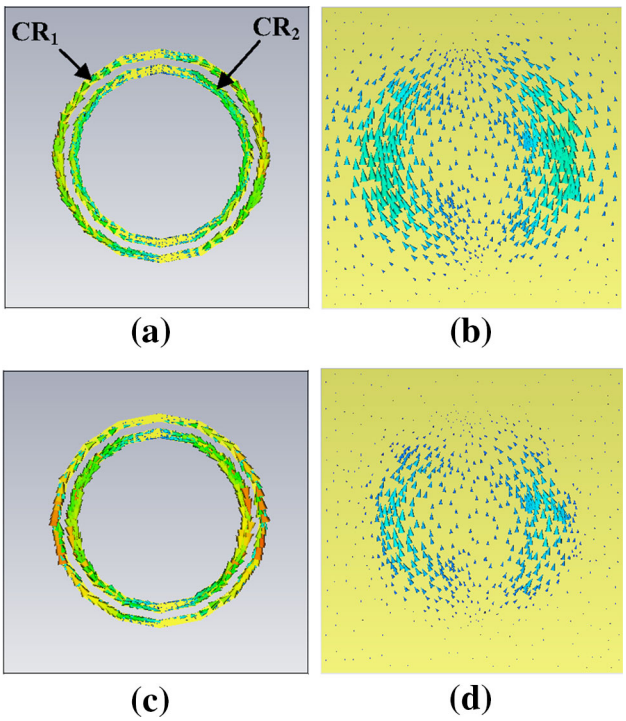

Fig. 11 Simulated surface currents at resonating elements: (**a**, **c**), and ground plane: (**b**, **d**) at two resonant frequencies. **a** $f = 9.00$ GHz, **b** $f = 9.00$ GHz, **c** $f = 11.00$ GHz, **d** $f = 11.00$ GHz

Similarly, the magnitude of E-field becomes weaker when approaching the horizontal part of the structure. Strong electric excitation that yields the electric resonant occurs. It happened at two resonant frequencies. The same behaviour is observed for H-Field as shown in Fig. 10b, d. Contrarily, the concentration of H-field distribution is high at the horizontal part of the structure along the incident magnetic field.

Next, investigation is continued by observing the surface currents of the dual-resonant CRMMAbs at the resonating elements and also bottom ground plane. As expected, anti-parallel surfaces current are observed between the top resonating elements and bottom ground plane as shown in Fig. 11. However, the patterns of surface currents at the ground plane are more dispersed, and the area is larger for lower resonant compared to the higher resonant. From this observation, it is proved that counter-circulating displacement currents exist in dielectric substrate between two metallic layers which are also coupled with the incident magnetic field. It yields a strong magnetic excitation within the structure that contributes to magnetic absorption.

Then, the surface currents flow is observed for individual resonating elements and combined elements. It is observed that the counter-circulated currents flow is formed in CR_1 and CR_2 at its own resonant frequency. It proves that electric excitation is existing. However, when

comparing the flow of currents simultaneously for both resonating elements, the direction of the currents flow is always anti-parallel at resonant frequencies. Thus, it proves that an electric wall is created between two resonating elements that yield a capacitive coupling. It will contribute to an electric absorption. The dominant resonating elements for each resonant frequency can be clearly observed by the magnitude and concentration of "cones" that refer to the currents flow. The magnitude and concentration of currents are high at CR_1 for 9 GHz while for 11 GHz at CR_2. The combination of electric and magnetic excitation forms electric quadruple response at two resonant frequencies that yield a strong electromagnetic absorption.

3 Conclusion

In conclusion, this paper presents the design and analysis of dual-resonant MMAbs that can work for dual-directional application. The combination of two circular rings with different sizes provides dual-resonant frequency absorption. Since the resonating elements are very symmetric in nature, this kind of MMAbs is polarization-insensitive. To determine the operating angle of the structure for oblique incident angle, the structure is simulated in both TE and TM polarizations. The operating angle of the structure is very large which is 70° and 67° for TE and TM polarizations, respectively. The fabrication and measurement are conducted to validate the simulated results. It is found that mutual agreement is achieved between simulated and measured result with slight frequency shift and ripples.

Acknowledgments The authors thank the Ministry of Higher Education (MOHE) for supporting the research work; Research Management Centre (RMC), School of Postgraduate Studies (SPS), Communication Engineering Department, Faculty of Electrical Engineering (FKE) and Universiti Teknologi Malaysia (UTM) Johor Bahru for the support of the research under Grant Nos. 4F360 and 05H35.

References

1. S. Lee, N. Kim, S.-Y. Rhee, in Design of novel artificial magnetic conductor as reflector and its SAR analysis. *Progress in Electromagnetics Research Symposium* (2012), pp. 325−328
2. J.F. Wang, S.B. Qu, Z.T. Fu, H. Ma, M. Yang, X. Wu, Three-dimensional metamaterial microwave absorbers composed of coplanar magnetic and electric resonators. Prog. Electromag. Res. Lett. **7**, 15–24 (2009)
3. N.I. Landy, S. Sajuyigbe, J.J. Mock, D.R. Smith, W.J. Padilla, Perfect metamaterial absorber. Phys. Rev. Lett. **100**, 207402 (2008)
4. W. Guo-Dong, L. Ming-Hai, H. Xi-Wei, K. Ling-Hua, C. Li-Li, C. Zhao-Quan, Multi-band microwave metamaterial absorber based on coplanar Jerusalem crosses. Chin. Phys. B **23**(1), 017802 (2014)
5. F. Hu, L. Wang, B. Quan, X. Xu, Z. Li, Z. Wu, X. Pan, Design of a polarization insensitive multiband terahertz metamaterial absorber. J. Phys. D Appl. Phys. **46**, 195103 (2013)
6. X.-R. Guo, Z. Zhang, J.-H. Wang, J.-J. Zhang, The design of a triple-band wide-angle metamaterial absorber based on regular pentagon close-ring. J. Electromag. Waves Appl. **27**(5), 629–637 (2013)
7. Y.J. Kim, Y.J. Yoo, K.W. Kim, J.Y. Rhee, Y.H. Kim, Y. Lee, Dual broadband metamaterial absorber. Opt. Express **23**(4), 3861–3868 (2015)